

**THE INITIAL TEMPERATURE AND N₂ DILUTION EFFECT ON THE
LAMINAR FLAME SPEED OF PROPANE/AIR**

**ZHENWEI ZHAO, ANDREI KAZAKOV, JUAN LI,
AND FREDERICK L. DRYER**

QUERY SHEET

- Q1 Au: Not listed in refs
- Q2 Au: pls. give article title
- Q3 Au: Give report titles; separate into three different references
- Q4 Au: Title of paper? Dates of meeting?
- Q5 Au: Please give author name(s) and access date of URL
- Q6 Au: Give title of journal
- Q7 Au: Please give title of thesis
- Q8 Au: Give title of paper, location & date(s) of meeting
- Q9 Au: Give title of paper

THE INITIAL TEMPERATURE AND N₂ DILUTION EFFECT ON THE LAMINAR FLAME SPEED OF PROPANE/AIR

**ZHENWEI ZHAO, ANDREI KAZAKOV, JUAN LI,
AND FREDERICK L. DRYER***

5

Department of Mechanical and Aerospace Engineering,
Princeton University, Princeton, New Jersey, USA

Laminar flame speeds of propane/air mixtures were determined experimentally over an extensive range of equivalence ratios at room temperature, 500 K, 650 K, and atmospheric pressure. Nitrogen addition to simulate effects of exhaust gas dilution on the laminar flame speed was also studied at these conditions for selected equivalence ratios. The experiments employed the stagnation jet-wall flame configuration in which the flow velocity was obtained by using particle image velocimetry. The laminar flame speed was obtained using linear extrapolation to zero stretch rate. The measured flame speeds were compared with literature data and numerical predictions using a published detailed kinetic model (Qin, Z., Lissianski, V., Yang, H., Gardiner, W. C., Jr., Davis, S. G., and Wang, H., *Proc. Combust. Inst.*, vol. 28, pp. 1663–1669, 2000). The predictions generally agree well with the experimental data. Both the data and model predictions reveal a quasi-linear relationship between the laminar flame speed and the dilution ratio, contrary to the nonlinear correlations commonly suggested in the literature. The linear

10

15

20

Accepted 11 March 2004.

This work was supported by General Motors Corp. (GM) via GM Contract No. TCS07299 and by the Chemical Sciences, Geosciences and Biosciences Division, Office of Basic Energy Sciences, Office of Science, U.S. Department of Energy under Grant No. DE-FG02-86ER13503. The authors also wish to acknowledge Dr. Richard Blint from GM for his technical management of GM portions of this work. The technical contributions of Dr. Michele Angioletti and Mr. Paul Michniewicz in performing the experiments are also acknowledged.

*Address correspondence to fldryer@princeton.edu

dependence issue is numerically extended to include hydrogen and methane flame systems.

Keywords: flame, laminar flame speed, initial temperature, dilution, propane 25

INTRODUCTION

Laminar flame speed data, as well as flame libraries that can be constructed from kinetic models validated against flame speed data, are critical input parameters for performing advanced numerical simulations, particularly for gasoline direct injection engines. Laminar flame speed 30 embodies the fundamental information on diffusivity, reactivity, and exothermicity of a given mixture and is therefore commonly used to characterize flames. As such, the measurement of laminar flame speed has received considerable attention in the published literature, particularly with regard to the effects of flame stretch on the fundamental (unstretched) laminar flame speed and the attainment of highly accurate, unperturbed measurements. Although accuracy is certainly a topic of 35 importance, repeatability and quantitative definition of flame speed variation with equivalence ratio, pressure, and inlet temperature are of principal interest in terms of applying laminar flame speed information to practical combustion system design. 40

Flame speed data have been reported in the literature from numerous sources and for various fuels burning in air at room temperature and pressure (e.g., Glassman, 1996). However, the extrapolation of these data 45 to initial temperatures, pressures, equivalence ratios, and dilution (or exhaust gas recirculation) levels important to engine combustion and to fuels utilized in engines is not simple. Although there are extensive data available for the laminar flame speed as a function of pressure, the data for different inlet temperature and/or diluents are relatively limited.

Here we present new measurements, using a modified version of the wall stagnation flame method to obtain additional data on propane/air 50 flames. Propane/air laminar reference flame speed measurements have been made with a wide variety of methods, and the more recent results in particular have become more or less a standard with regard to validating methodology. The specific objective of the present work was to experimentally 55 determine laminar flame speeds of propane/air mixtures over a range of equivalence ratios at room temperature, but also at initial gas temperatures of 500 and 650 K, with particular interest near lean

flammability and sooting limit conditions. Nitrogen addition (up to 40% by volume), to simulate the effects of exhaust gas dilution on laminar flame speed, was also studied for selected equivalence ratios and initial reaction temperatures (0.8 and 1.1 at 300 K, 1.1 at 500 and 650 K). In performing this work, we not only wished to validate the method modifications that we implemented and provide new experimental data to augment that in the literature, but to further discuss the accuracy issues associated with reference laminar flame experimental determinations. Finally, robust kinetic mechanisms specifically developed for flame speed predictions are now available in the literature (Qin et al., 2000). Here we show the consistency of computational predictions with the new measurements, including the effects of unburned gas temperature and dilution.

EXPERIMENTAL METHODOLOGY

The experimental configuration used, a single jet-wall stagnation flame, was introduced by Egolfopoulos et al. (1997) and is discussed in more detail elsewhere (Zhao, 2002). When the strain rate is low, the flame front is far away from the nonadiabatic stagnation plate; therefore, the downstream heat loss has a minimal effect on the flame propagation. Figure 1 shows the schematic of the experimental setup. The setup includes a stagnation plate under which a premixed flame burner is located. The premixed reactant flow emerges upward from the 14-mm converging nozzle situated at the center of a water/N₂-cooled burner surface and impinges vertically onto a 3.5-in.-diameter thin ceramic flat plate. The material used is silica foam, which has much lower conductivity and heat capacity than stainless steel. This material provides near-adiabatic conditions but continues to result in radiative loss of gas temperatures in close contact with the plate surface. The burner flow is shrouded by a 2-mm annular flow of nitrogen to stabilize the flame. The flowfield disturbances resulting from the shroud flow and duct exit-to-wall distance (25 mm) were shown to be negligible, experimentally.

The airflow first goes into a seeder to pick up particles for the particle image velocimetry (PIV), and then the flow is preheated by using an inline heater. Finally the flow is mixed with gaseous fuel in a turbulent mixer. The residence time upstream of the burner where all components are premixed and at the appropriate initial temperature is minimized to

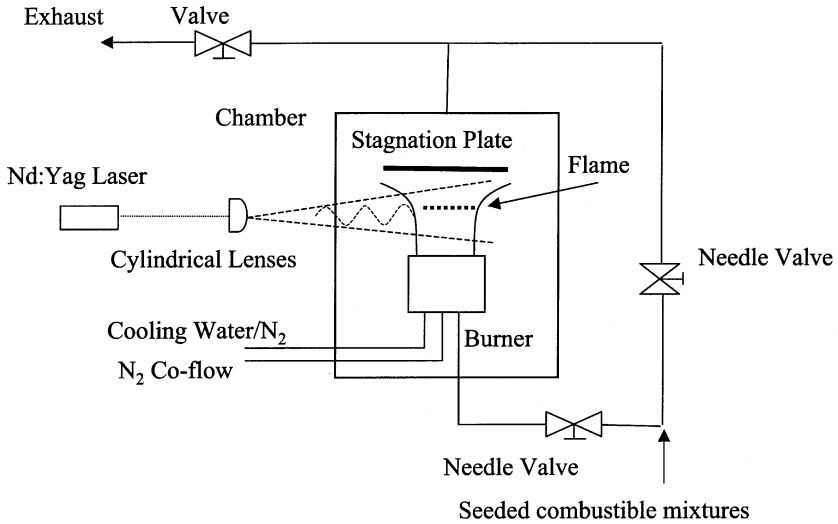


Figure 1. Schematics of the experimental setup.

prevent two-stage ignition flashback at high preheat. The mixture is then separated into two parts by using two high-temperature needle valves. One part of the mixture goes into the burner and the other part goes into the exhaust, thus allowing the variation of the burner flow velocity without manipulating the individual flow rates of each component. The body of the burner is heated by flexible Omega[®] rope heaters capable of accommodating the irregular shapes around inlets and outlets. The N₂ coflow was preheated by another inline heater to keep its temperature the same as that of the main flow. The burner is insulated with a ceramic blanket. The heaters, mixer, and needle valves are installed in an insulated box to maintain near-isothermal conditions.

The temperature of the air/gas inline heaters is closed-loop controlled using a phase-angle-fired power controller. Several 1.6-mm exposed-junction fast-response thermocouples are used to measure local temperatures. The final temperature of the mixture, which is measured 3.8 mm away from the nozzle exit and under the screen of the nozzle, is used as the control temperature. The location of the temperature sensor is based on trade-off considerations among minimizing flame radiation effects, flow disturbance, and proximity to the flame location itself.

The entire burner system is housed within a cylindrical (27 cm height × 41 cm o.d.) chamber to contain exhaust gases. Four symmetrically

located chamber exhausts reduce the perturbation compared to a single exhaust. Three optical windows in the chamber wall are purged with preheated N_2 to keep the windows clear of pollutants and condensation. The chamber is insulated on its interior with aluminum oxide and purged with nitrogen through a porous metal cover to reduce flame perturbations. The exhaust is cooled by additional N_2 flow and a water-coil heat exchanger prior to entering a scrubber to remove the particles upstream of the lab exhaust system. 120

The flow is seeded with 0.3–0.7 μm boron nitride particles, and the velocity of the entire flow field can be obtained using PIV. Particles of diameter 0.3–0.7 μm and mass density of the present material have been shown by many studies (e.g., Egolfopolous and Campbell, 1999; Mei, 1996; Mei et al., 1991; Sung et al., 1996) to track similar flows with even higher strain rates (e.g., turbulent combustion and opposite jet flames measurement) closely. A Continuum[®] Minilite PIV Nd:Yag laser is used as the PIV light source and the light beam is shaped into a thin light sheet using cylindrical and spherical lenses. The images at two different times are recorded by double exposure using a Kodak DCS 460 digital camera with resolution of 3060×2036 pixels. The recorded images, in appropriate digital form, are subsequently analyzed using an in-house autocorrelation code. The PIV code utilizes self-optimizing fast Fourier transform algorithms, variable interrogation window size, and subpixel peak detection techniques. In addition, customized filtering algorithms implemented in the code facilitate autodetection of the flow centerline and the flame edge, thus allow the processing of large data sets (reducing statistical experimental errors) with minimal user interaction. Additional features include algorithms for automatic interrogation peak selection/rejection as well as stretch rate/reference flame speed determination. The use of this software package eliminates human bias in determining the stretch rate manually, which is a technique commonly reported for the laser Doppler velocimetry (LDV)/PIV-related flame speed studies appearing in the literature. 125 130 135 140 145

The uncertainties in velocity measurements using any optical method that tracks particle motion depend on the statistics gathered from multiple events as well as the optical interrogation cell window within which the sampling occurs. In the case of PIV, there is a trade-off between seeding density and interrogation window size. Although increasing the size of the window improves the statistics, it may also limit the spatial resolution of the PIV-determined velocity since the average particle 150 155

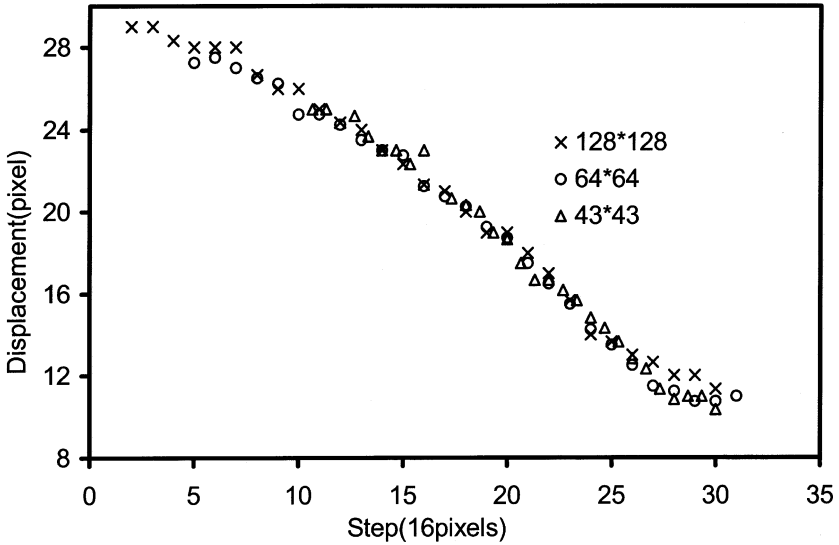


Figure 2. Effect of autocorrelation window size on the observed displacement.

velocity within the window may be skewed. Figure 2 presents the particle displacement determined at fixed time interval for the same image as a function of interrogation window size. As window size is decreased, seeding must be increased to maintain a sufficient number of particles within the window to achieve appropriate statistical sampling. It was found that a 64×64 pixel interrogation cell was sufficiently small to yield good spatial resolution without inordinate degradations in statistical sampling.

160

RESULTS AND DISCUSSION

Flame Speed and Stretch Rate Determined by PIV

165

PIV can determine the velocity map of the entire two-dimensional flow field. The particle density and displacement between two exposures were chosen for the optimal application of the autocorrelation technique. Because of thermal expansion and flow acceleration immediately upstream of the flame front, the particle density becomes too low to obtain reliable vectors using autocorrelation. However, this characteristic also results in a very well-defined flame front location (Hirasawa et al., 2001; Zhao et al., 2001). The minimum point in the axial velocity profile

170

was defined as the reference flame speed while the stretch rate for each measurement was determined from the quasi-linear part of the axial velocity profile upstream. Although using a constant-temperature location in the flame profile might be conceptually a more proper reference condition (Tien and Dixon-Lewis, 1990; Matalon, 1991), given the uncertainties introduced by the need for temperature profile measurements, the velocity minimum reference method continues to be commonly employed. (e.g., Davis and Law, 1998; Hirasawa et al., 2002). Linear extrapolation was used to determine the zero-stretched laminar flame speed from a plot of the reference flame speed versus the stretch rate. The direction of the velocity in a stagnation flow is well defined, thus avoiding a directional ambiguity issue characteristic of the autocorrelation approach.

Q1

The presence of the stagnation wall in the jet-wall setup allows the determination of flame speeds at considerably lower strain rates than are typical of data obtained using the opposed-jet configuration (Hirasawa et al., 2001). Lower strain rates are critical to obtaining a reliable extrapolation, since the strain rate and flow velocity determinations each have statistical experimental uncertainties. Figure 3 shows an example of the measured stretch rate as a function of the reference flame speed. The data exhibit a degree of scatter comparable to that reported in similar studies (Hirasawa et al., 2001). Caution should be taken when comparing just the visual appearance of the data scatter obtained from PIV and LDV measurements. The PIV measurements provide single-event snapshot images. In LDV, however, each individual data point is already time-averaged, which tends to reduce the apparent scatter. As discussed before, the statistical averaging used in the present work can reduce the induced uncertainty caused by the scatter in the raw data, and the uncertainty in the definition of stretch rate, which is one of the largest sources of error in the stagnation flame method (Hirasawa et al., 2001). Although the automatic determination of the stretch rate used in the present work is more systematic, it may result in an apparent greater degree of scatter, which would otherwise appear smaller as a result of human bias present in manual data reduction.

Uncertainty Analysis

In the present work, the fluctuation in the gas flow rates is less than 1% and yields an uncertainty in the equivalence ratio of ± 0.01 . The

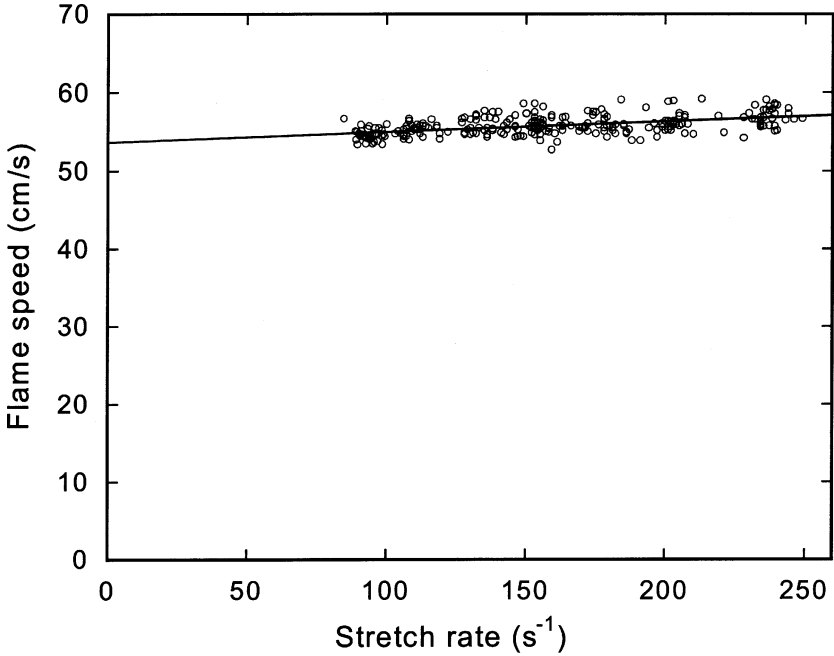


Figure 3. Example of linear extrapolation used to determine the laminar flame speed (initial temperature 500 K, with 25.48% N₂ dilution).

uncertainty in the flow velocity obtained from the PIV method by using subpixel peak identification is about ± 0.1 pixels (Westerwell et al., 1997; Willert and Gharib, 1991), yielding an uncertainty in the measured velocity of $\pm 1.25\%$. However, statistical averaging used in the present work can reduce this uncertainty, because it is random error. Therefore, the largest uncertainty in the determined laminar flame speed is introduced by the linear extrapolation process, which is often overlooked in the literature. In the present work, a conventional regression analysis is used to estimate this uncertainty. From statistical theory (Draper and Smith, 1986), the uncertainty can be estimated using the following equations:

$$E_{\text{prd}} = t_{(\alpha/2, n-2)} s \sqrt{1 + \frac{1}{n} + \frac{(x_p - \bar{x})^2}{\sum (x_i - \bar{x})^2}} \quad (1)$$

215

220

$$E_{\text{slp}} = \frac{t_{(\alpha/2, n-2)} S}{\sqrt{\sum (x_i - \bar{x})^2}} \quad (2)$$

where E_{prd} is the uncertainty in the predicted flame speed, E_{slp} is the uncertainty in the slope of stretch rate versus flame speed (i.e., Markstein length), and

$$s = \sqrt{\frac{\sum (y_i - y_i')^2}{n - 2}}$$

is approximately equal to the standard deviation. The coefficient t is a function of both α , the confidence limit, and n , the total number of the data points. In the present experiments, 95 and 68.27% confidence intervals correspond to $t \approx 2$ or 1, respectively; x_i and y_i represent the observed strain rate and reference flame speed, respectively; \bar{x} is the mean value of strain rate; x_p is the strain rate at which the flame speed is to be predicted (i.e., zero); and y_i' is the value of flame speed at the i th point estimated from the linear relation. For the experimental results presented here, the uncertainty evaluated using Eq. (1) is less than 5%.

There are three general ways to reduce the uncertainty in flame speed determination caused by extrapolation: (1) increase the precision of individual observations, which will decrease the standard deviation; (2) obtain lower strain rate measurements, that is, reduce the range of extrapolation; and (3) increase the number of experimental data points. The following analysis illustrates the importance of obtaining low strain rate data, an issue that motivated the choice of the experimental configuration used in the present work.

By using Eq. (1), an analysis of the linear extrapolation and associated uncertainty shows that the extrapolation itself is the major source of error, especially when the number of data points is small and the lowest experimentally observed stretch rate is high. To compare the uncertainty in our data with that of other measurements appearing in the literature (Vagelopolous and Egolfopoulos, 1998; Vagelopolous et al., 1994), the uncertainty associated with different lowest experimentally observed stretch rate values and with different number of measurement points is shown in Figure 4. For example, if the raw experimental data have a 2.5% standard deviation, the lowest experimentally observed stretch rate of 300 s^{-1} , and 16 measurements used in the extrapolation,

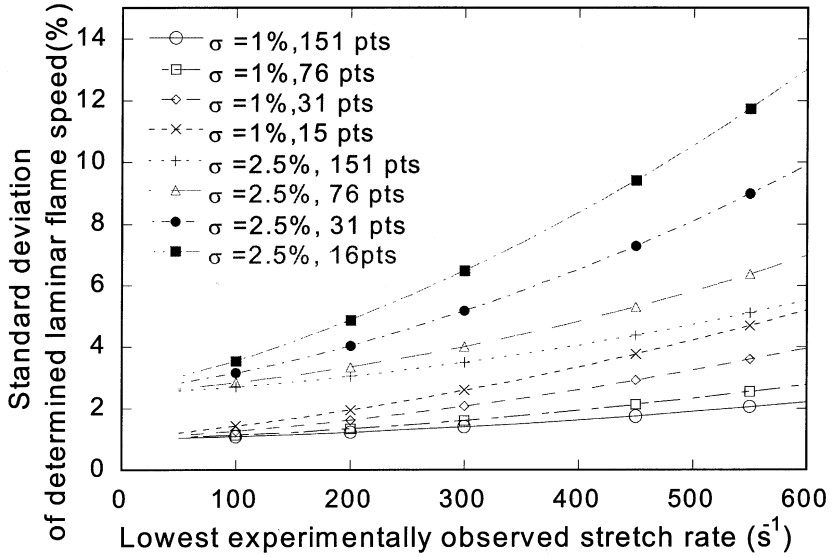


Figure 4. Effect of the lowest experimentally observed stretch rate on the uncertainty in the determined laminar flame speed caused by linear extrapolation.

the uncertainty in the determined laminar flame speed is 6.5%. Using 1200 raw data points in the extrapolation, the uncertainty in determined laminar flame speed will be 3.0%. On the other hand, the same number of raw data points and uncertainties, but a lowest experimental observed stretch rate of 100 s^{-1} , result in determined laminar flame speed uncertainties of 2.8% (16 points) and 2.6% (1200 points). A 95% confidence interval requires a doubling of all of the uncertainty values just mentioned. These examples illustrate that the uncertainty in the flame speed determined by any extrapolation is always larger than the standard deviation of raw flame speed data. Furthermore, the uncertainty is always reduced by decreasing the lowest stretch rate of experimental measurements. The published literature has typically reported only standard deviation in the raw flame speed data and has not commented on the uncertainties in the determined laminar flame speed arising from the extrapolation itself. These arguments apply regardless of whether linear or nonlinear extrapolation is adapted.

Similarly, by using Eq. (2), the uncertainty of the slope of the stretch rate versus the stretched flame speed (i.e., the Markstein length) has also been analyzed with respect to different uncertainty of the stretched flame

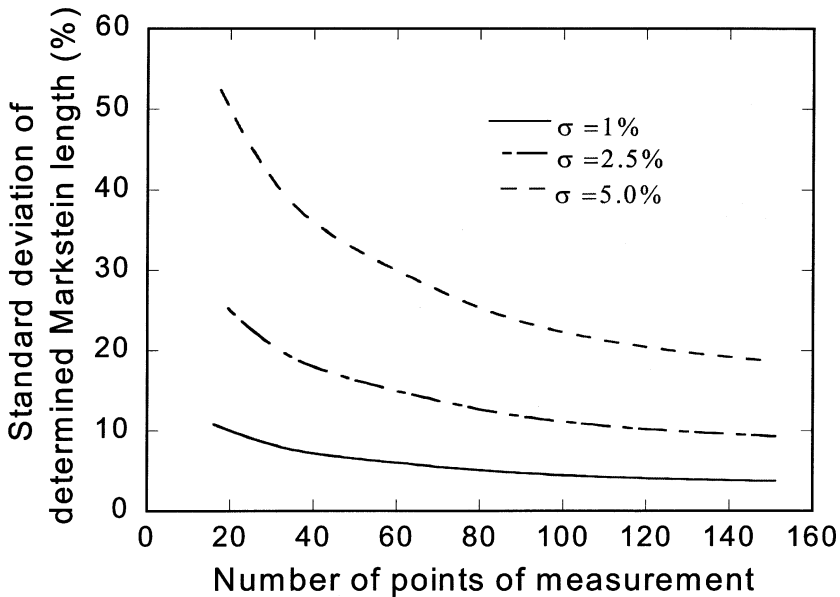


Figure 5. Effect of the number of experimental points on the uncertainty in the determined Markstein length (σ is the standard deviation of the observation).

speed or stretch rate with different numbers of experimental observations (Figure 5). It is clear that the uncertainty in the Markstein length increases with the standard deviation of individual measurements of the flame speed and the stretch rate and decreases with the number of measurement points. One can also see that for the same set of experimental data the uncertainty of the determined Markstein length is usually much larger than that of the determined flame speed; for example, with 2.5% standard deviation for 16 points of measurement, the standard deviation of the determined Markstein length is 27.1%. This large uncertainty in Markstein length is one of the causes of the differences in the literature-reported value of this parameter.

RESULTS

Figure 6 shows the measured propane/air mixture flame speeds for different equivalence ratios at room temperature. Other literature data (Dugger, 1952; Metghalchi and Keck, 1980; Vagelopolous and Egolfopoulos, 1998; Vagelopolous et al., 1994) are also presented.

The overall agreement among different data sets is generally very good, and the present data agree within 4% with the most recent measurements by Vagelopoulos et al. 1994; Vagelopoulos and Egolfopoulos, 1998)

Figure 6 also shows the comparison of the experimental data with laminar flame speed predictions using the detailed reaction mechanism of Qin et al. (2000). The Qin et al. mechanism was originally optimized against ignition delay and room temperature flame speed data for a number of C_1 - C_3 hydrocarbon fuels. The laminar flame speed was computed with the PREMIX (Kee et al., 1985) code of the Sandia CHEMKIN II package (Kee et al., 1989). We implemented an optically thin radiation submodel in the PREMIX code to assess the effects associated with radiative heat losses. The Planck mean absorption coefficients for H_2O , CO_2 , CH_4 , and CO were taken from the Sandia web site (International Workshop, 2003). The inclusion of radiative heat losses resulted in extremely small (less than 0.1 cm/s) differences in the predicted flame speeds, even for the cases with high (650 K) unburned gas

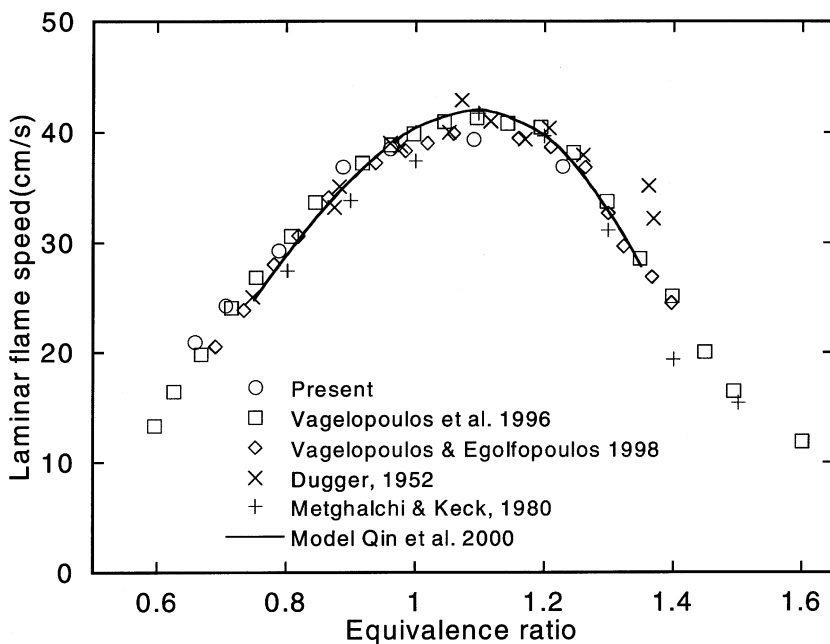


Figure 6. Atmospheric pressure, room temperature laminar flame speeds for propane/air mixtures.

temperatures. As can be seen, the predictions using the model of Qin et al. (2000) agree very well with the entire body of experimental data. The original mechanism development included the data of (Vagelopoulos et al., 1994; Vagelopoulos and Egolfopoulos, 1998) in the optimization but no cases at other unburned gas temperatures or with dilution. 310

Figure 7 compares the present data at different unburned gas temperatures, 500 and 650 K, with the predictions using the same model. Model calculations again show good overall agreement with the data; however, the deviations become significant at the lean limit and on the rich side for the 650 K case. 315

Figure 8 displays the present data in comparison to the limited data available in the literature on the effect of varying initial gas temperature. Our results appear to be consistent with the extensive data set of Dugger (1952) taken at seven different unburned gas temperatures (ranging from 200 to 616 K) using the Bunsen burner apparatus, and the data of Desoky et al. (1990) at 433 K obtained with the spherical bomb method. The data extracted from the temperature-dependent spherical bomb measurements 320

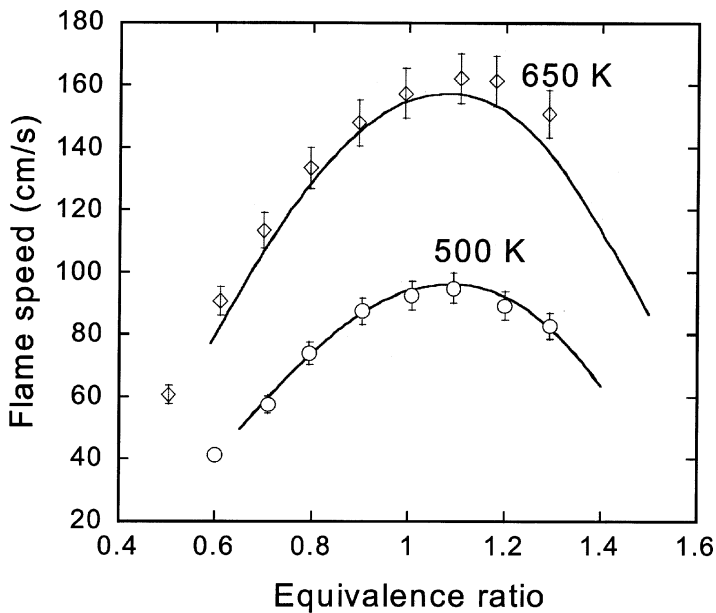


Figure 7. Atmospheric pressure laminar flame speeds for propane/air mixture at 500 and 650 K. symbols, experimental data; lines, model (Qin et al., 2000) predictions.

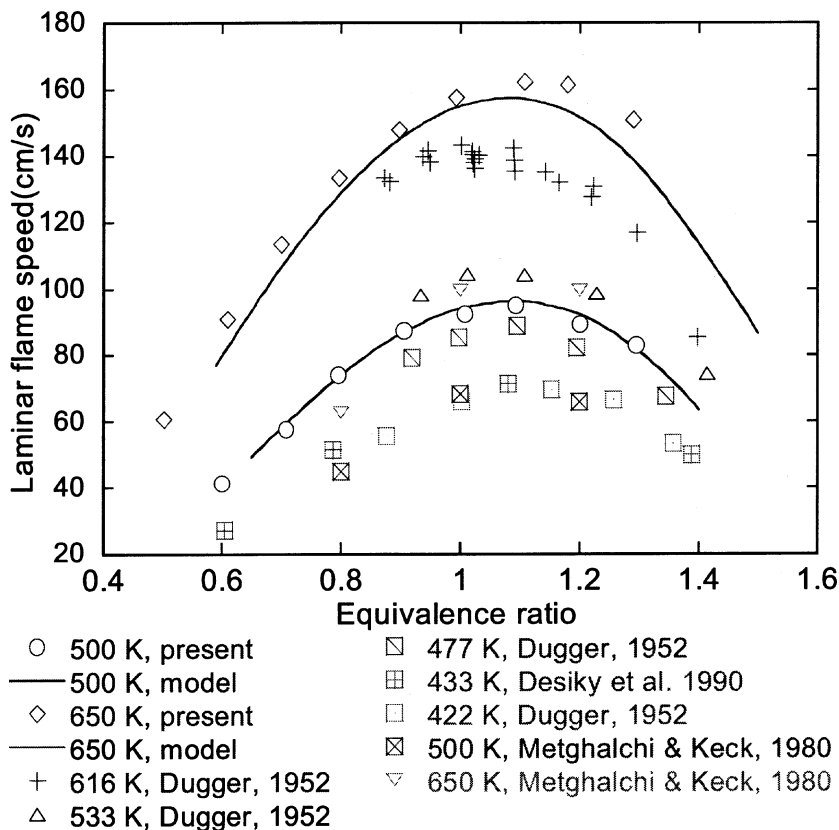


Figure 8. Comparison of atmospheric pressure laminar flame speed of preheated propane/air mixtures.

of Metghalchi and Keck (1980) at 500 and 650 K are considerably lower than those from the present study, with differences up to 38%.

Figure 9 shows the experimental results for propane/air mixture with N_2 dilution. The dilution ratio is defined here as the diluent volume over the total volume (diluent + air + fuel) expressed as a percentage. For the cases considered in the present study, that is, three different unburned gas temperatures (300, 500, and 650 K) and the dilution levels from 0 to up to 40%, the measured laminar flame speeds exhibit nearly linear dependencies with respect to the dilution ratio up to the flammability limit. Moreover, the theoretical results obtained using the same reaction mechanism agree very well with the experiments and confirm the same

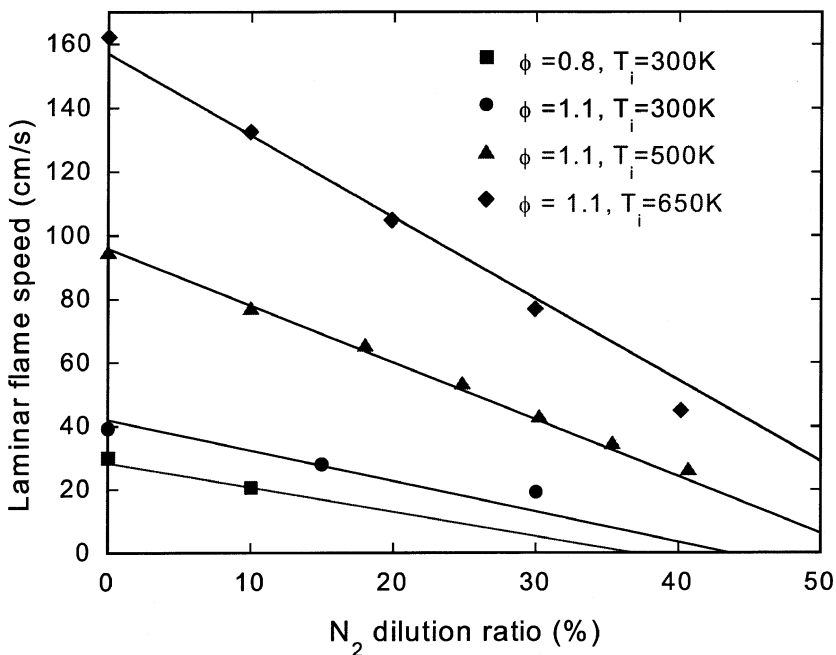


Figure 9. Variation of laminar flame speed at atmospheric pressure with N₂ dilution for equivalence ratio 0.8 at 300 K, and 1.1 at 300, 500, and 650 K. The symbols represent the present experimental data, and lines represent the model (Qin et al., 2000) predictions.

trend. This result clearly contradicts the nonlinear nature of the correlation between the laminar flame speed and the dilution ratio, even at relatively low levels of dilution commonly suggested in the literature (e.g., Fells and Rutherford, 1969; Haniff et al., 1989, Stone et al., 1998; van Oostendorp et al., 1990). To further illustrate the effect of dilution on the flame speed, the laminar flame speed of C₃H₈ at other equivalence ratios was also computed using the same kinetic model. In addition, the behavior of flame speed versus N₂ dilution ratio for CH₄/air/N₂ and H₂/air/N₂ mixtures have also been tested numerically by using the same C₁-C₃ reaction mechanism (Qin et al., 2000) and the recent hydrogen oxidation model of Li et al. (2003), respectively. The results are presented in Figure 10. For all the fuels studied (C₃H₈, CH₄, and H₂), the flame speed decreases quasi-linearly (within ±2% deviation) with the dilution ratio up to the flammability limit. Due to the simplified treatment of radiative heat transfer used in the present calculations, the predictions at

340

345

350

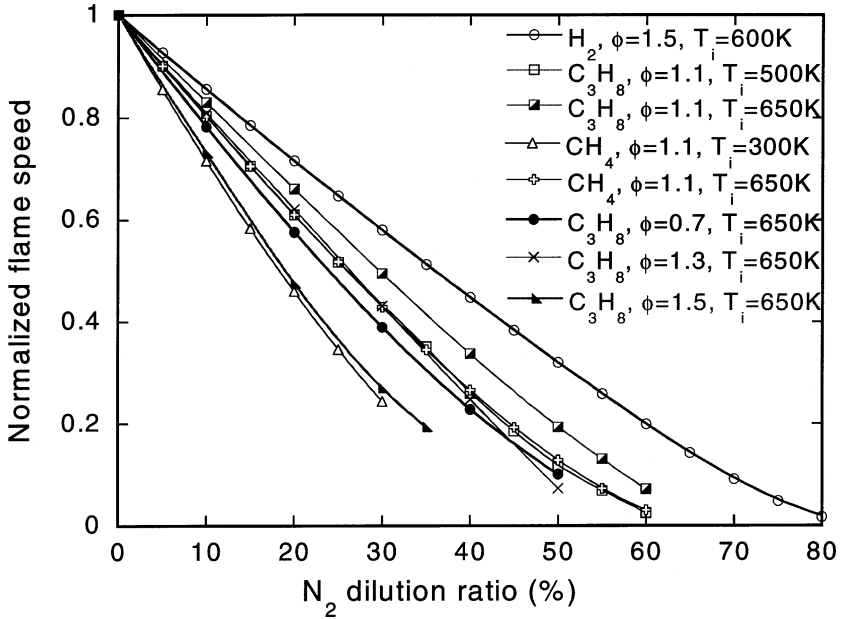


Figure 10. Predicted laminar flame speed of H_2 , CH_4 , and C_3H_8 as a function of N_2 dilution ratio. The data are normalized by the value obtained at zero dilution.

the conditions close to the flammability limit (and the flammability limits themselves) are not expected to be very accurate. Nevertheless, it is clear that within the practical dilution range the laminar flame speed exhibits a nearly linear dependence with respect to the N_2 dilution ratio at all equivalence ratios for all three fuels. In addition, the same trend has been recently shown experimentally and numerically for gasoline/air/ N_2 mixtures (Zhao et al., 2003). Based on extensive experimental and numerical information we have developed, the dependence of the laminar flame speed on the dilution ratio essentially is quasi-linear and different in slope in comparison to prior results appearing in the literature. To further facilitate the development of more accurate correlations, the computed slopes of the linear correlations between the laminar flame speed and the dilution ratio for C_3H_8 flames are presented in Figure 11 as functions of equivalence ratio and unburned gas temperature. The absolute value of the slope increases significantly with the initial temperature and slightly varies with equivalence ratio ϕ . For a fixed initial temperature, the absolute value of the slope reaches its maximum and

355

360

365

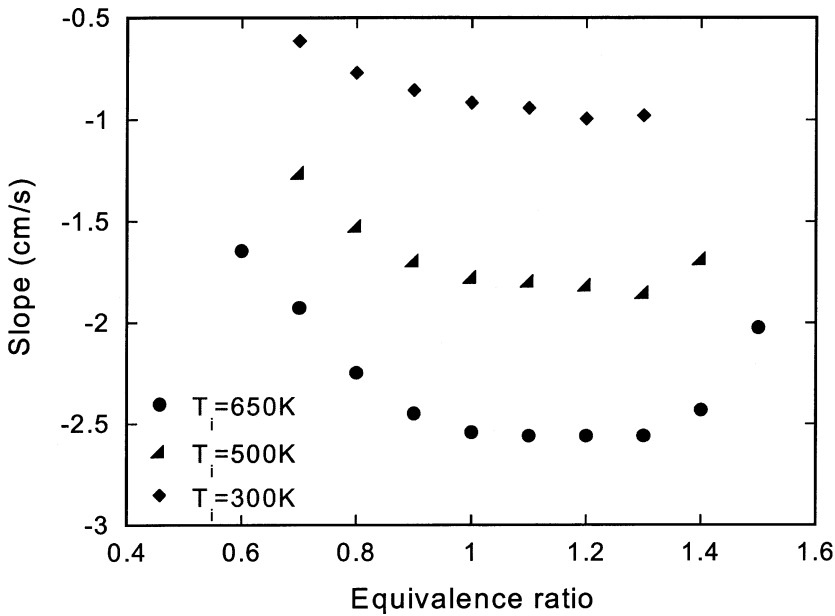


Figure 11. Computed slopes of the linear correlations between the laminar flame speed and the dilution ratio for C_3H_8 flames.

changes little over the range of $\phi = 1.1$ – 1.3 , while increasing with ϕ for $\phi < 1.1$ and $\phi > 1.3$. The observed functions vary smoothly with respect to their parameters and can be easily and accurately parameterized for further use in practical applications. 370

CONCLUSIONS

Laminar flame speeds for propane/air mixtures at atmospheric pressure with mixture initial temperature of 300, 500, and 650 K were determined on a stagnation flame using PIV. The measured values agree well with modeling results based on a recent detailed reaction mechanism of propane oxidation (Qin et al., 2000), with a significant difference on the rich side of 650 K. Both the data and model predictions have revealed a linear relationship between the laminar flame speed and the dilution ratio, contrary to the nonlinear correlations commonly suggested earlier. 380

REFERENCES

- Q2 Desoky, A.A., Abdel-Ghafar, Y.A., and El-Badrawy, R.M. (1990) *Int. J. Hydrog. Energy*, **15**, 895–905.
- Q2 Dixon-Lewis, G. (1990) *Symp. Int. Combust.*, **23**, 305–324. 385
- Draper, N.R. and Smith, H. (1986) *Applied Regression Analysis*, John Wiley and Sons, New York.
- Dugger, G.L. (1952) NACA Report 1061, NACA Technical Note 2170, NACA Technical Note 2374.
- Q3
- Q2 Egolfopoulos, F.N., Zhang, H., and Zhang, Z. (1997) *Combust. Flame*, **109**, 237–252. 390
- Q2 Egolfopoulos, F.N. and Campbell, C.S. (1999) *Combust. Flame*, **117**, 206–226.
- Q2 Fells, I. and Rutherford, A.G. (1969) *Combust. Flame*, **13**, 130–138.
- Glassman, I. (1996) *Combustion*, 3rd ed. Academic Press, San Diego.
- Q2 Haniff, M.S., Melvin, A., Smith, D.B., and Williams, A. (1989) *J. Inst. Energy*, **62**, 229–236. 395
- Hirasawa, T., Sung, C.J., Yang, Z., Wang, H., and Law, C.K. (2001) *2nd Joint Meeting of the U.S. Section of the Combustion Institute*, Oakland, Paper No. 138.
- Q4
- Q2 Hirasawa, T., Sung, C.J., Joshi, A., Yang, Z., Wang, H., and Law, C.K. (2002) *Proc. Combust. Instit.*, **29**, 1427–1434. (2003). 400
- Q5 International Workshop on Measurement and Computation of Turbulent Nonpremixed Flames. Radiation Models. <http://www.ca.sandia.gov/TNF/radiation.html> (accessed xxx).
- Q4
- Kee, R.J., Grcar, J.F., Smooke, M.D., and Miller, J.A. (1985) *A Fortran Program for Modeling Steady Laminar One-Dimensional Premixed Flames*. Sandia Report SAND85-8240, Sandia National Laboratories, Albuquerque, NM. 405
- Kee, R.J., Rupley, F.M., and Miller, J.A. (1989) *CHEMKIN II: A Fortran Chemical Kinetics Package for the Analysis of Gas Phase Chemical Kinetics*. Sandia Report SAND89-8009, Sandia National Laboratories, Albuquerque, NM. 410
- Q4 Li, J., Zhao, Z., Kazakov, A., and Dryer, F.L. (2003) *2003 Technical Meeting of the Eastern States Section of the Combustion Institute*, paper no. 43.
- Q2 Mei, R. (1996) *Exp. Fluids*, **22**, 1–13.
- Q2 Mei, R., Adrian, R.J., and Howard, P.J. (1991) *J. Fluid Mech.*, **225**, 481–495. 415
- Q2 Metghalchi, M. and Keck, J.C. (1980) *Combust. Flame*, **38**, 143–154.
- Q2 Qin, Z., Lissianski, V., Yang, H., Gardiner, W.C., Jr., Davis, S.G., and Wang, H. (2000) *Proc. Combust. Instit.*, **28**, 1663–1669.
- Q2 Stone, R., Clarke, A., and Beckwith, P. (1998) *Combust. Flame*, **114**, 546–555.
- Q2 Sung, C.J., Kistler, J.S., Nishioka, M., and Law, C.K. (1996) *Combust. Flame*, **105**, 189–201. 420
- Q2 Tien, J.H. and Matalon, M. (1991) *Combust. Flame*, **84**, 238–248.

- Q2 Vagelopolous, C.M. and Egolfopoulos, F.N. (1998) *Symp. Int. Combust.*, **27**, 513–519.
- Q2 Vagelopolous, C.M., Egolfopoulos, F.N., and Law, C.K. (1994) *Symp. Int. Combust.*, **25**, 1341–1347. 425
- van Oostendorp, D.L. and Levinsky, H.B. (1990) *J. Inst. Energy*, **63**, 160–166.
- Q2 Westerwell, J., Dabiri, D., and Gharib, M. (1997) *Exp. Fluids*, **23**, 20–28.
- Q6 Q2 Willert, C.E. and Gharib, M. (1991) **10**, 181–193.
- Q7 Zhao, Z. (2002) M.S. Thesis, Mechanical and Aerospace Engineering Department, Princeton University, Princeton, NJ. 430
- Q8 Zhao, Z., Kazakov, A., and Dryer, F.L. (2001) *2001 Technical Meeting of the Eastern States Section of the Combustion Institute*, pp. 416–419.
- Q9 Zhao, Z., Conley, J.P., Kazakov, A., and Dryer, F.L. (2003) SAE paper 2003-01-3265. 435